ADVANCES IN ATMOSPHERIC SCIENCES, VOL. 24, NO. 5, 2007, 781–798

Seasonal Phase-Locking of Peak Events in the Eastern Indian Ocean

Qin ZHANG* and Song YANG

RS Information System, Climate Prediction Center, National Weather Service/National Oceanic and Atmospheric Administration, Camp Springs, MD 20746*, USA*

(Received 8 October 2006; revised 18 December 2006)

ABSTRACT

The sea surface temperature (SST) anomaly of the eastern Indian Ocean (EIO) exhibits cold anomalies in the boreal summer or fall during El Niño development years and warm anomalies in winter or spring following the El Niño events. There also tend to be warm anomalies in the boreal summer or fall during La Niña development years and cold anomalies in winter or spring following the La Niña events. The seasonal phase-locking of SST change in the EIO associated with El Niño/Southern Oscillation is linked to the variability of convection over the maritime continent, which induces an atmospheric Rossby wave over the EIO. Local air-sea interaction exerts different effects on SST anomalies, depending on the relationship between the Rossby wave and the mean flow related to the seasonal migration of the buffer zone, which shifts across the equator between summer and winter.

The summer cold events start with cooling in the Timor Sea, together with increasing easterly flow along the equator. Negative SST anomalies develop near Sumatra, through the interaction between the atmospheric Rossby wave and the underneath sea surface. These SST anomalies are also contributed to by the increased upwelling of the mixed layer and the equatorward temperature advection in the boreal fall. As the buffer zone shifts across the equator towards boreal winter, the anomalous easterly flow tends to weaken the mean flow near the equator, and the EIO SST increases due to the reduction of latent heat flux from the sea surface. As a result, wintertime SST anomalies appear with a uniform and nearly basin-wide pattern beneath the easterly anomalies. These SST anomalies are also caused by the increase in solar radiation associated with the anticyclonic atmospheric Rossby wave over the EIO. Similarly, the physical processes of the summer warm events, which are followed by wintertime cold SST anomalies, can be explained by the changes in atmospheric and oceanic fields with opposite signs to those anomalies described above.

Key words: seasonal phase locking, ENSO monsoon interaction

DOI: 10.1007/s00376-007-0781-7

1. Introduction

Previous studies have identified an anomalous pattern of the Indian Ocean (IO) sea surface temperature (SST) with a strong seasonal character (e.g., Wolter and Hastenrath, 1989). Recent discussions about the Indian Ocean dipole (IOD) mode (Saji et al., 1999; Webster et al., 1999) have stimulated a renewed interest in investigating the ocean-atmosphere interaction over the ocean. Saji et al. (1999), based on an empirical orthogonal function (EOF) analysis of IO SST, proposed a secondary dipole mode and claimed that the mode was independent from El Niño/Southern Oscillation (ENSO). Indeed, the IOD index, and the difference in SST between the eastern Indian Ocean (EIO; 10°S–0°, 90°–110°E) and the western Indian Ocean (WIO; 50°–70°E, 10°S–10°N), was correlated strongly with the time series of the second EOF mode of SST and the zonal wind over the central IO, but poorly with the Niño-3 SST index.

More careful analyses indicate that, while some dipole events occur in non-El Niño years (e.g., 1961 and 1967) or weak El Niño years (e.g., 1994), others take place in El Niño developing years (1972, 1982 and 1997). Some studies (e.g., Saji et al., 1999; Webster et al., 1999) emphasize one side of the IOD-ENSO relationship and suggest that the IOD mode could develop independently from ENSO. On the other hand, many others have argued that the variability of IOD was linked to the conditions of ENSO. For exam-

*Corresponding author: Qin ZHANG, qin.zhang@noaa.gov

ple, Yu and Rienecker (1999) and Murtugudde et al. (2000) analyzed the oceanic process during 1997–98 and concluded that the cooling in EIO and the warming in WIO were related to ENSO events. It was also generally claimed that the dominant modes of interannual variability of IO SST were closely associated with ENSO (Anderson and McCreary, 1985; Cadet, 1985; Nigam and Shen, 1993; Tourre and White, 1995; Nicholson, 1997; Wu and Meng, 1998; Chambers et al., 1999; Venzke et al., 2000; Yoo et al., 2006).

Allan et al. (2001) also questioned the weakness of IOD for causing significant climate signals. The changes in atmospheric circulation over the IO are primarily related to the large-scale fluctuations of the Southern Oscillation, a seesaw in sea level pressure between the central Pacific and northern Australia (Bjerknes, 1969; Barnett, 1983; Rasmusson and Wallace, 1983), which is linked to many anomalies of atmospheric circulation over the IO. During El Niño years, the zonal circulation over the tropical IO is weakened by the suppression of convection over the maritime continent, through both the atmospheric bridge (Lau and Nath, 1996) and the Indonesian throughflow (Wyrtki, 1987; Meyers, 1996; Yamagata et al., 1996; Potemra and Lukas, 1999). As pointed out by Krishnamurthy and Kirtman (2003), a significant fraction of the variability of SST in the tropical Indian and Pacific oceans was related to ENSO. They argued that SST anomalies of the same sign appeared in the eastern Pacific and WIO from December to May and a so-called dipole structure developed from June to November in the tropical IO.

The fluctuations of the tropical IO SST are complex because they are not only determined by ocean dynamics but also influenced by the Asian monsoon, ENSO, and local air-sea interaction. However, the variability of IO is also marked by certain oscillatory features (Huang and Kinter, 2002; Yang et al., 2007) and characteristic processes of changes in the atmosphere and ocean (Yu and Rienecker, 1999; Xie et al., 2002; Loschnigg et al., 2003; Saji and Yamagata, 2003). Indeed, in the tropical IO, maximum SST variability appears in the EIO. As it will be seen later, this SST variability plays an important role in explaining the basin-wide IO SST anomalies. On the contrary, the SST anomalies in the equatorial WIO are much weaker than those in the tropical southeastern IO. Furthermore, the WIO anomalies do not develop simultaneously with those in the southeast, which are more likely linked to ENSO (Venzke et al., 2000; Krishnamurthy and Kirtman, 2003; Yu et al., 2003). These differences in SST variability between the EIO and WIO and their relationship with the IOD cause difficulties in explaining the external and internal forcing factors of the IOD, and for discussing the robustness of the phenomenon and its physical process (Allan et al., 2001; Baquero et al., 2002; Dommenget and Latif, 2002, 2003; Yamagata et al., 2003; Shinoda et al., 2004). This is particularly so because the dipole-like pattern only appears in an unrotated EOF analysis, but not in the rotated EOF and simple regression analyses, suggesting that it could be an artifact of the specific method being used and might not necessarily correspond to physically meaningful modes (Dommenget and Latif, 2002, 2003). As argued by Hastenrath (2002), the IOD pattern can at most be interpreted as a change in the zonal SST gradient, instead of an east-west SST seesaw.

In this study, we attempt to shed light on the variability of the EIO SST and the physical mechanisms responsible for the SST variability and improve our understanding of the relationship between the IO SST and ENSO. We focus on the warm and cold events of the EIO SST and identify these events based on the seasonal peak phase of SST anomalies. We first describe the data and methodology in Section 2. We then document the basic features and time evolution of the cold and warm events in Section 3. The physical mechanisms responsible for these events are discussed in Sections 3 and 4. Next, we discuss the relationship between the tropical EIO SST and ENSO, in Section 5. The last section summarizes the results, along with a discussion of several key issues related to the subject of this study.

2. Data and method

The datasets used in this study include the Extended Reconstructed Sea Surface Temperature (ERSST; Reynolds and Smith, 1994), the NOAA's Climate Prediction Center Merged Analysis of Precipitation (Chen et al., 2003), and the National Centers for Environmental Prediction (NCEP)—National Center for Atmospheric Research (NCAR) reanalysis (Kalnay et al., 1996). In particular, the wind fields and surface heat fluxes (latent heat flux, sensible heat flux, downward solar radiation, and net heat flux) from the NCEP-NCAR reanalysis product are analyzed. Note that surface heat fluxes are type C variables in the reanalysis and there may be uncertainties in the obtained surface heat flux anomalies.

Version 7 of the retrospective analysis of the global ocean, based on the Simple Ocean Data Assimilation (SODA) data (Carton et al., 2000a,b), is also used to diagnose the oceanic process during the cold and warm EIO events. The data are available in monthly means, in a $1^\circ \times 1^\circ$ latitude-longitude horizontal resolution from January 1958 to December 2000. The SODA

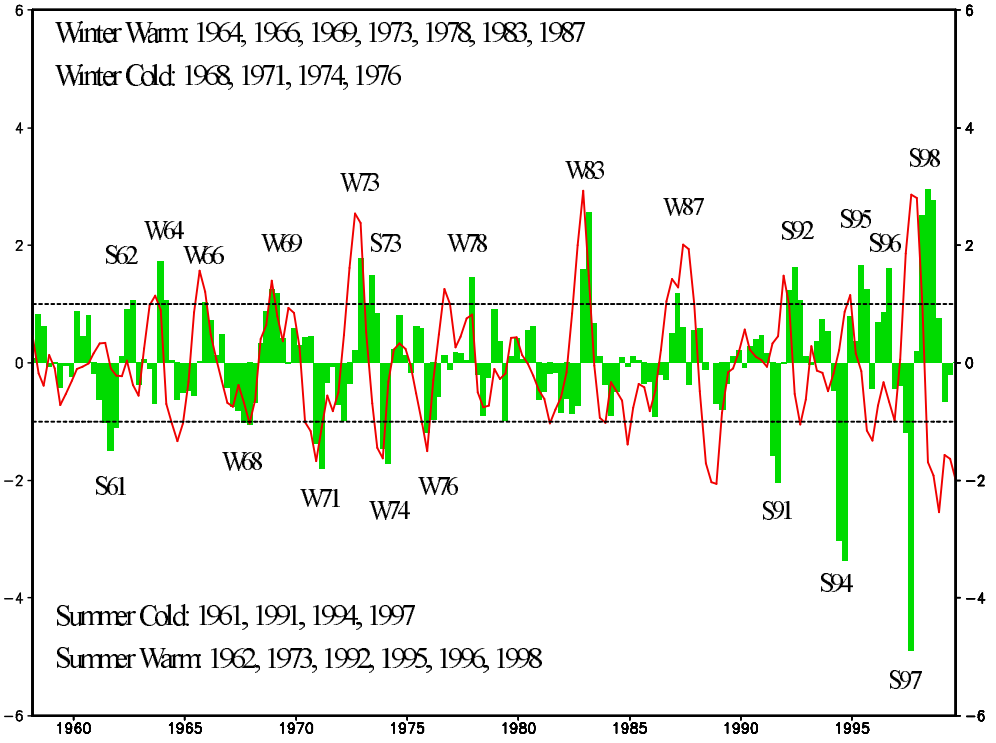

Fig. 1. Normalized seasonal means of SST anomalies averaged over the EIO (0°–10°S; 90°–110°E, bars) and Niño-3.4 region (5°S–5°N; 170°–120°W, line) from January 1958 to December 1999. The two dashed lines indicate the locations of one standard deviation.

Table 1. A list of cold and warm EIO seasons defined by the values exceeding one standard deviation of the SST anomalies over (0°–10°S, 90°–110°E). The winter (summer) events include the conditions of DJF and MAM (JJA and SON). The years shown in parentheses are not included in the cold and warm events because their values peak in the prior or subsequent years (see Fig. 1).

	Cold EOI Seasons	Warm EOI Seasons
DJF	1962, 68, 71, 74, 76	1964, 66, 69, 73, 78, 83
MAM	1971, 74	1964, 69, 73, 83, 87, 92, 98
JJA	1961, 91, 94, 97	1973, 92, 95, 98
SON	1961, 67, 91, 94, 97	1962, 92, 95, 96, 98
Winter Events (DJF/MAM)	(1962), 68, 71, 74, 76	1964, 66, 69, 73, 78, 83, 87, (92), (98)
Summer Events (JJA/SON)	1961, (67), 91, 94, 97	1962, 73, 92, 95, 96, 98

analysis has been constructed using optimally-interpo lated data assimilation combining numerical model forecasts with temperature and salinity profiles, SST, and altimeter sea level. The first-layer sea temperature of SODA is highly correlated with the ERSST, with a coefficient of 0.75 for the region (0°–10°S, 90°–110°E).

For all data fields, we remove the signals longer than seven years, including the linear trends, by an harmonic analysis. Since we are to focus on the features of cold and warm categories and their relationship with ENSO, and because of the phase-locking of these features to the annual cycle, we apply a composite technique in our analysis. In addition, we use the one-sample and two-sample student t-tests to assess the statistical significance of the results obtained.

3. Evolution of the cold and warm events in the eastern Indian Ocean

In the EIO, the standard deviation of SST, which is the highest in the tropics (> 0.5°C), exhibits two peaks: one in February and the other in October (figures not shown). For the period 1958–99, the correlation between the SST averaged over (0°–10°S, 90°–110°E) (EIO) and the Niño-3.4 SST is +0.45 when the EIO lags Niño-3.4 by six months, and −0.3 when the EIO leads Niño-3.4 by five months. The simultaneous correlation between the two is highest in February

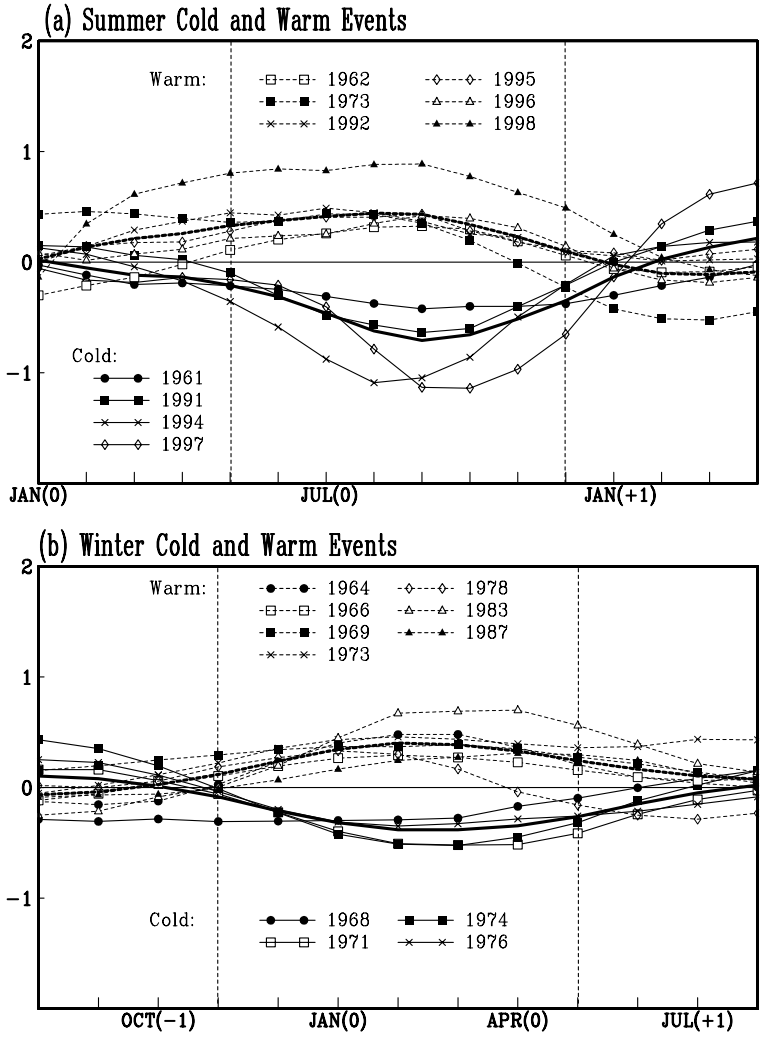

Fig. 2. EIO SST anomalies (°C) (a) for four cold cases (solid lines) and six warm cases (dashed lines) of the summer events, and (b) for four cold cases (solid lines) and seven warm cases (dashed lines) of the winter events. The thick solid and dashed lines measure the composite values for each group. Values between the two vertical dashed lines show significance at the 95% confidence level. The numbers 0, −1, and +1 in the x-coordinate denote the current, prior, and post year of the events, respectively.

(0.7) and October (−0.5). These features indicate that negative SST anomalies appear in the EIO two months before the El Niño mature phase (usually in December) and positive SST anomalies emerge two months after the El Niño mature phase.

We define the cold and warm EIO events by the SST anomalies exceeding one standard deviation and select the events according to the information provided in both Table 1 and Fig. 1. Specifically, Table 1 presents a list of cold and warm EIO seasons and Fig. 1 shows the standardized SST anomalies over the EIO and Niño-3.4 region. We classify these events into two groups: summer events, if the maximum SST anomaly appears in the boreal summer (June-July-August: JJA) or fall (September-October-November: SON); and winter events, if the maximum anomaly occurs in the boreal winter (December-January-February: DJF) or spring (March-April-May: MAM). As indicated in Fig. 1, the summer events include four cold cases (1961, 1991, 1994, and 1997) and six warm cases (1962, 1973, 1992, 1995, 1996, and 1998), and winter events include four cold cases (1968, 1971, 1974, and 1976) and seven warm cases (1964, 1966, 1969, 1973, 1978, 1983, and 1987). The years of

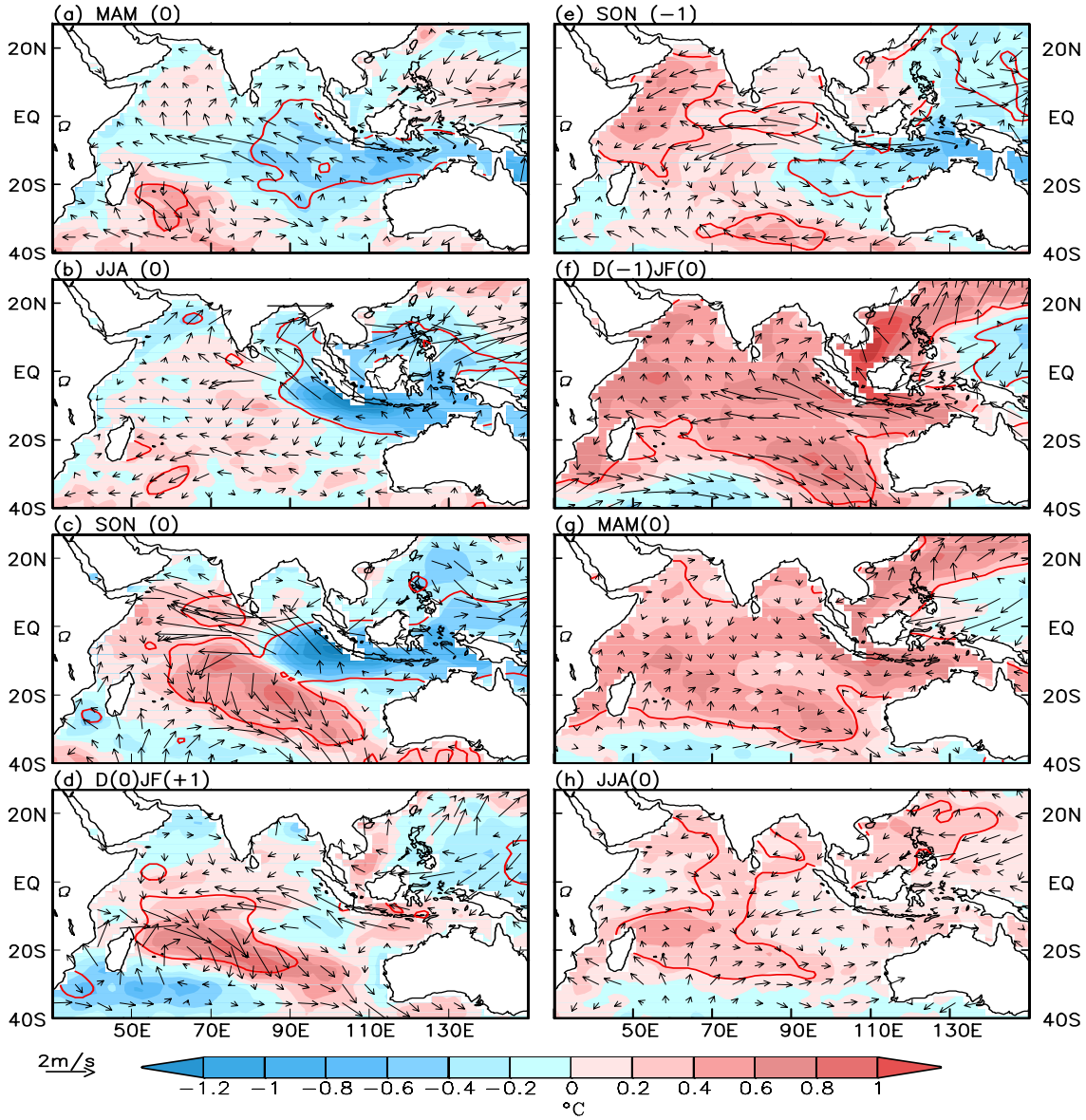

Fig. 3. Composite patterns of the differences in seasonal surface winds (arrows; m s^{-1}) and SST (shading; °C) for the summer (cold minus warm; left panels) and winter (warm minus cold; right panels) events. The red lines show the regions where the differences in SST are significant at the 95% confidence level.

1962, 1992 and 1998 have not been selected to the winter events because the peak SST anomalies appeared in the preceding summers. Similarly, the year of 1967 has not been selected to the summer events because the peak SST anomalies appeared in the subsequent winter (1968).

As shown in Fig. 2a, the summer events start to develop in spring and decay after November (see the vertical dashed lines). Between the seven-month lifespan from May to November, the signals exceed significantly the 95% confidence level, based on the two-sample student t-test. The composite values (thick lines) show that the cold events reach their mature phase in September but the warm events peak one month earlier, in August. Most of the summer cold events (except 1961) occur in El Niño developing years and all of the summer warm events lead the cold SST anomaly in the eastern Pacific (La Niña) by 3–6 months. The amplitude of the cold events is stronger than that of the warm events, implying that oceanic processes may play an important role in the development of cold SST anomalies in the EIO (Murtugudde et al., 2000; Yu et al., 2003; also, see the discussion in section 4).

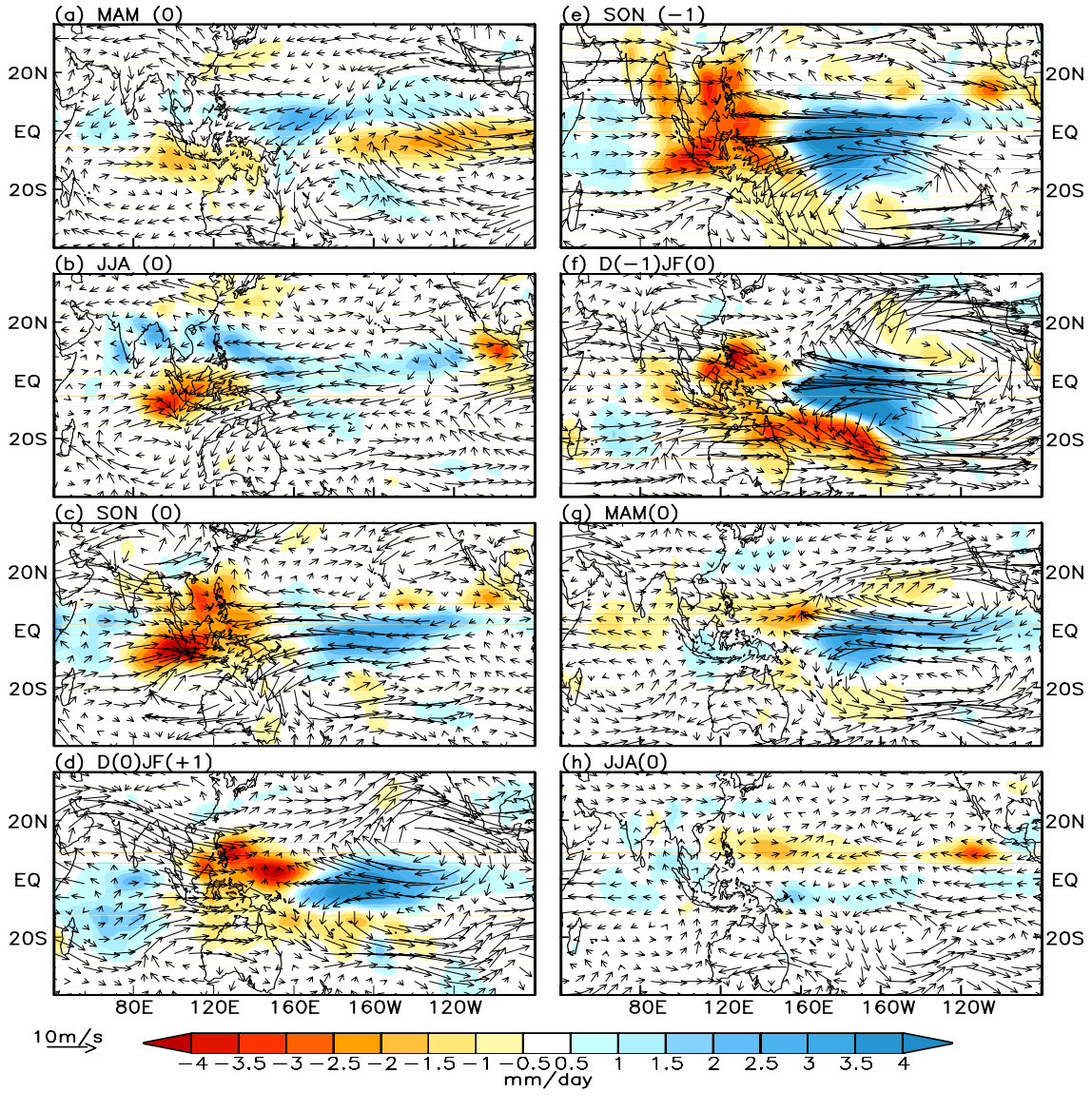

Fig. 4. Composite patterns of the differences in seasonal 200-hPa winds (arrows; m s^{-1}) and precipitation (shading; mm d^{-1}) for the summer (cold minus warm; left panels) and winter (warm minus cold; right panels) events.

Figure 2b displays the evolution of the winter warm and cold events in the EIO. These events begin in November of the prior year and end in April with a lifespan of six months, characterized by maximum SST anomalies in February. Most of the winter warm (cold) events occur in El Niño (La Niña) decay years, except the 1968 and 1987 events.

The EIO cold and warm events are tightly phase-locked to the annual cycle, so we construct composite patterns to investigate their evolution processes. Figure 3 shows the differences in seasonal surface winds and SST for the summer (cold minus warm; left panels) and winter events (warm minus cold; right panels). For the cold events, negative SST anomalies appear over both the tropical EIO and the maritime continent in MAM (Fig. 3a), with a center near the Timor Sea. These SST anomalies, whose significant portion (highlighted by the solid lines) may be initially linked to the Pacific SST anomaly by the atmospheric bridge (Lau and Nath, 1996), or by the Timor Passage of the Indonesian throughflow (Wyrtki, 1987; Meyers, 1996), develop strongly near Sumatra in JJA (Fig. 3b), with a large temperature gradient established along the equator. They reach a mature phase in October (Fig. 3c) and rapidly decay in the subsequent DJF (Fig. 3d). Another striking feature is the warm center extending

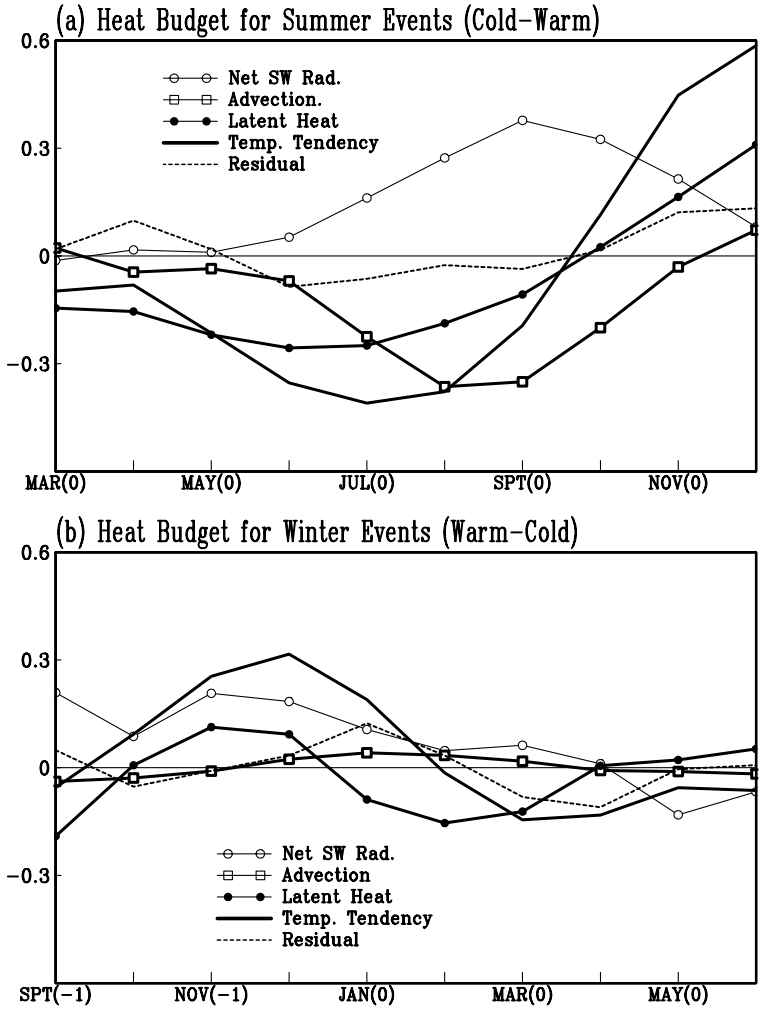

Fig. 5. Composite of the differences in SST tendency (solid black lines), net solar radiation (lines with open circle), latent heat flux (lines with closed circle), oceanic advection contribution to SST changes (lines with open square), and residual (dashed black lines) averaged over (0°–10°S, 90°–110°E). Values are shown for both summer events (a; cold minus warm) and winter events (b; warm minus cold). Unit: °C month^{-1}.

from the southern-central IO to the WIO during SON and DJF, as shown in Figs. 3c–d. The evolution of the summer cold events is similar to that of the IOD, but the largest SST anomalies appear in the central-southern IO, instead of the western equatorial region.

Associated with the cold SST signal in the EIO are the anomalous easterly wind near the equator and the southeasterly wind along Java and the Sumatra coast. These anomalous winds appear in MAM and intensify and form an anticyclonic pattern over the southeastern IO in JJA (also see Wang et al., 2003). Note that the anomalous easterly flow and the anomalous anticyclone last persistently until DJF when the cold SST signal becomes very weak and even disappears.

The evolution of the summer warm events is similar, but the SST and surface wind anomalies change oppositely to those shown above. In the EIO, the SST warming is not as strong as the cooling discussed previously. Warm events reach their peak one month earlier than the cold events, indicating that the asymmetric development of the cold and warm events may result from the effect of oceanic dynamics (Clarke and Liu, 1993).

Figures 3e–h show the evolution of the winter events. The basin-wide warm (cold) SST anomalies develop after the El Niño (La Niña) mature phase by two to three months. Easterly (westerly) anomalies exist over the EIO and anticyclonic (cyclonic) anomalies appear over the southeastern IO in SON and DJF (Figs. 3e–f). The uniform SST pattern is the principal

component of the interannual variation of the IO SST, which is strongly correlated with the Niño-3.4 SST of three months earlier, as shown by Nicholls (1989), Kiladis and Diaz (1989), Hastenrath et al. (1993), Ju and Slingo (1995), Latif and Barnett (1995), and Venzke et al. (2000).

Therefore, the summer cold events are characterized by cold SST anomalies in the EIO (as well as in the Bay of Bengal and northern Arabian Sea) and warm anomalies in most of the central and western tropical IO, with a cold center in the equatorial southeastern IO and two warm centers in the southern IO and WIO, respectively. Easterly anomalies are persistent along the equator, accompanied by an anticyclonic pattern over the southeastern IO. In the winter warm events, SST anomalies of uniform sign occur in the entire tropical IO, with anomalous winds along the equator and anticyclonic anomalies over the southern IO. The changes in winds are similar to those of the summer cold events. The summer warm events and the winter cold events are associated with physical processes described by correspondingly opposite signs in the anomalies of SST and atmospheric circulation. Most of the winter warm (cold) events that correspond to El Niño (La Niña) and reach their mature phase in December or January have experienced cold (warm) SST anomalies in the EIO in the prior summer and fall when El Niño (La Niña) is in the development phase. From 1958 to 1999, about 65% of the interannual variation of tropical IO SST can be explained by the cold and warm events in summer and winter.

Consistent features can also be found in the precipitation and 200 hPa wind fields (Fig. 4). In the summer cold cases, precipitation decreases over the maritime continent but increases over the tropical western Pacific in MAM (Fig. 4a). Towards JJA, precipitation is further suppressed over the maritime continent (Fig. 4b). The reduction in convective heating generates a baroclinic anticyclonic (cyclonic) Rossby wave at the lower (upper) troposphere (Gill, 1980) over the southeastern IO and produces anomalous easterlies near the equator and southeasterlies along the west coast of Australia and Sumatra Islands at the lower troposphere (see Fig. 3). Meanwhile, precipitation increases over the Philippine Sea, the South China Sea, and the central equatorial Pacific, associated with the development of ENSO (Meehl, 1997; Wang et al., 2000).

The reduction in precipitation over the maritime continent and EIO continues in SON (Fig. 4c). A pair of atmospheric Rossby waves is clearly seen over the tropics of both the southern and northern hemispheres, caused by the suppressed convection. By now, the upper-level anomalous cyclone over the southeastern IO shifts eastward, and active convection develops over the WIO while convection is suppressed over the equatorial southeastern IO. In the meantime, precipitation increases over the central Pacific, exciting another pair of atmospheric Rossby waves over the northern and southern tropics (Nitta and Yamada, 1989; Wang and Zhang, 2002). This feature indicates that ENSO is towards its full development. The deficit of precipitation over the maritime continent persists to DJF (Fig. 4d) when precipitation appreciably characterizes the Australian monsoon and the cold SST anomalies over the EIO decay significantly (see Fig. 3d).

The features of winter warm events (Figs. 4e–f) are similar to those discussed above except that larger amplitude appears in the boreal winter. Indeed, when precipitation decreases over the maritime continent and increases over the central Pacific, the IO SST is characterized by a dipole pattern in the boreal summer and fall (figures not shown), which evolves to a uniform pattern in the boreal winter and spring. The change in convection over the maritime continent plays a key role in regulating the interannual variability of IO SST through the induced atmospheric Rossby wave over the EIO, which interacts strongly with the underneath ocean in different monsoon backgrounds between summer and winter.

4. Diagnosis of top ocean layer SST anomalies

In order to assess quantitatively the contributions of different atmospheric and oceanic processes to the changes in EIO SST, we examine the various terms of the equation for top-layer temperature. As descriptions in studies of Lau and Nath (2004), Wang et al. (2003) and Murtugudde et al. (2000), the changes in temperature are determined by the anomalous advection in the top ocean layer and the net heat flux across the air-sea interface, and can be expressed as follows when the ocean advection is linearized about the time mean:

$$\frac{\partial T'}{\partial t} = -\left(\boldsymbol{V}\cdot\nabla T\right)' - \left(W\frac{\partial T}{\partial z}\right)' + \frac{1}{\rho c_p H}\left(Q_{\mathrm{SW}} + Q_{\mathrm{LW}} + Q_{\mathrm{LH}} + Q_{\mathrm{SH}}\right)', \qquad (1)$$

where the prime represents temperature anomalies from the time mean. The first two terms on the right-hand side of the equation represent the anomalous horizontal and vertical oceanic advection. $\boldsymbol{V}$ and W are, respectively, the horizontal (zonal and meridional) and vertical components of the top-layer ocean current. The last term of the equation is the anomalous

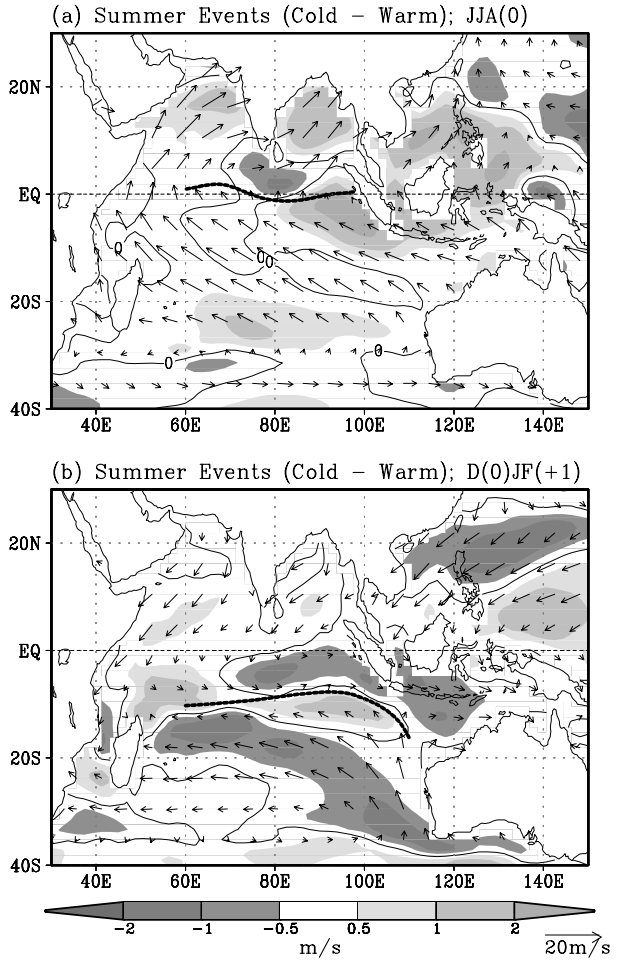

Fig. 6. (a) JJA means of climatological surface winds (vectors) and the difference in wind speed (shading) for summer events (cold minus warm). (b) Same as in (a), but for the subsequent DJF. The thick dashed lines indicate the transition zones between easterlies and westerlies. Units: m s^{-1}.

net heat flux exchanged between oceans and the atmosphere. ρ and c_p are the density and specific heat of ocean water, respectively. H is the thickness of the top ocean layer, Q_{SW} and Q_{LW} represent the shortwave and longwave components of radiation at the ocean surface, and Q_{LH} and Q_{SH} are the surface latent and sensible heat fluxes. Since longwave radiation and sensible heat flux are much smaller than the other two flux terms, they are ignored in the further analysis. Note that other complex processes including subsurface vertical transport, vertical mixing, and horizontal diffusions, are considered a residual and thus not discussed in this study.

Figure 5 shows the composite SST tendency averaged over (0°–10°S, 90°–110°E) for the summer and winter events, together with solar radiation, latent heat flux, oceanic advection contribution, and the residual. To estimate the contributions of ocean dynamic processes to the changes in SST, we calculate the anomalous temperature advection in the top ocean layer from the SODA data by assuming a mixed layer depth of 50 m and ignoring oceanic dissipation. In the summer cold events (Fig. 5a), the anomalous solar radiation and temperature advection are almost out of phase and thus offset each other. They lag the anomalous SST tendency by about 2–3 months, indicating that an increase in solar radiation is a negative feedback owing to less cloudiness caused by the anomalous anticyclone over the southeastern IO. On the other hand, the oceanic advection prevents a recovery of the cold SST anomalies to the normal condition and continues to decrease the local SST (Murtugudde and Busalachi, 1999). This feature explains why the summer cold events reach a peak phase one month later, in September, as described above. We will discuss how the oceanic dynamic process plays a role in detail later. It is notable that latent heat flux leads the anomalous SST tendency by one month, implying the importance of latent heat flux for the cooling or warming of the sea surface. The maximum cooling tendency occurs in JJA when the ocean loses more latent heat as the summer monsoon prevails over the tropical IO (see Fig. 6a later).

In the winter warm events (Fig. 5b), solar radiation and latent heat flux are the two main contributors to warm the sea surface of the EIO. The mechanism involving solar radiation-cloudiness-SST feedback can be easily understood for both summer and winter events because of the anomalous anticyclone over the EIO. However, the effect of latent heat flux is opposite between the summer and winter events, because of the air-sea interaction under the different backgrounds of summer and winter monsoons. We investigate the wind speed-evaporation-SST feedback process in the following subsection.

4.1 *Air-sea interaction under summer and winter monsoon backgrounds*

The equatorial easterly (westerly) anomalies over the IO, generated by the decrease (increase) in convection over the maritime continent, persist from summer to the next spring (see Fig. 4). One may wonder why the EIO SST anomalies decrease in summer before ENSO and increase in winter after ENSO. As pointed out above, latent heat flux is the key factor of the SST change over the EIO through local air-sea interaction under the different summer and winter monsoon backgrounds.

Latent heat flux Q_{LH} is linked to local wind speed and specific humidity by the bulk aerodynamic law:

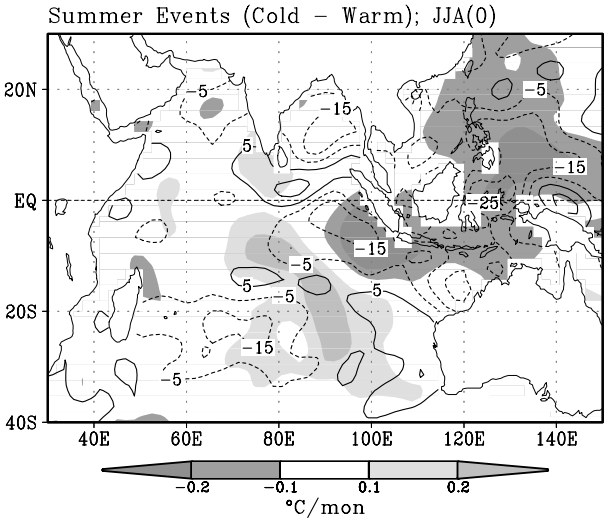

Fig. 7. JJA means of the differences in SST tendency (°C month^{-1}; shading) and latent heat flux (W m^{-2}; contours) for summer events (cold minus warm).

higher wind speed and lower humidity at the lower atmosphere increase latent heat loss from the ocean to the atmosphere and thereby cool the ocean surface. Before the onset of the Asian summer monsoon, winds are light along the equator over the IO (called monsoon buffer zone), where the northeasterly winter monsoon meets the southeasterly trade winds from the Southern Hemisphere. When the summer monsoon appears in late spring and early summer, the convectively inactive buffer zone, a sharp turning of winds near the equator, shifts northward and extends to the central-western IO. The southeasterly flow to the south of the buffer zone recurves northeastward over the WIO and crosses the equator, becoming a main branch of the southwesterly summer monsoon flow over the northern IO (Shukla, 1987).

Thus, the easterly anomalies enhanced by the anomalous anticyclonic winds over the southern IO decrease the southwesterly summer monsoon to the north of the buffer zone but increase the trade winds to the south of the buffer zone (see Fig. 6a). The wind-evaporation-SST positive feedback causes the ocean to lose more heat and decreases the SST to the south of the buffer zone. Therefore, cold events develop rapidly during the summer monsoon period. When the buffer zone shifts back to the south of 10°S in boreal winter, northwesterly flow prevails along the equator (Fig. 6b). The cold SST anomalies disappear rapidly since the anomalous easterly flow is in an opposite direction to the mean flow. The weakened winds prevent a further release of latent heat to the atmosphere under the winter monsoon background and the SST in the EIO recovers quickly to its normal condition.

Q_{LH} may also be affected by local oceanic conditions: the loss of latent heat to the atmosphere is reduced (enhanced) above a cold (warm) sea surface. However, this relationship is unclear from the composite charts for SST and Q_{LH} (see Fig. 5a), indicating that the influence of wind speed on Q_{LH} is relatively stronger for the summer events. Figure 7 shows the composite patterns of anomalous SST tendency and latent heat flux. It is seen that latent heat flux Q_{LH} is an important contributor to the pattern of SST tendency, suggesting that local air-sea interaction plays a critical role in determining the EIO SST pattern under the seasonally-varying monsoon background. However, the SST tendency does not match the latent heat flux very well in some places. For example, outside the specific regions such as that shown by Fig. 5 (0°–10°S, 90°–110°E), it is more difficult to interpret the features by the thermodynamic heating-SST relationship. Furthermore, latent heat flux becomes only the second most important component, after oceanic advection, for the summer events from July to the middle of September (Fig. 5a). This suggests a considerable contribution to the change of SST by oceanic dynamic processes, which will be discussed in the next subsection.

4.2 *Ocean dynamic processes in summer cold events*

It has been seen from Fig. 5b that, in the winter events, the anomalous temperature tendency caused by oceanic advection is small compared to the other terms. Because of this, we only discuss the oceanic dynamical processes for the summer events. We express the change of SST in the following form:

$$\frac{\partial T'}{\partial t} = -\boldsymbol{V}' \cdot \nabla \overline{T} - \overline{\boldsymbol{V}} \cdot \nabla T' - W' \frac{\partial \overline{T}}{\partial z} - \overline{W} \frac{\partial T'}{\partial z} + \frac{1}{\rho c_p H}(Q'_{\mathrm{SW}} + Q'_{\mathrm{LH}}) \qquad (2)$$

The first and third terms on the right-hand side ($-\boldsymbol{V}' \cdot \nabla \overline{T}$ and $-W' \partial \overline{T}/\partial z$) represent the action of anomalous current on the time-mean temperature; whereas $-\overline{\boldsymbol{V}} \cdot \nabla T'$ and $-\overline{W} \partial T'/\partial z$ indicate the effects of the mean current on temperature anomalies. The spatial distributions of these four linearized advection terms are displayed in the right panels of Fig. 8. In the computations, we use $\boldsymbol{V}', W'$, and T' to represent the anomalous summer conditions, and use $\overline{\boldsymbol{V}}, \overline{W}$, and $\overline{T}$ to represent the climatological means. To facilitate the interpretation of these results, we follow Lau and Nath (2004) and show the distributions of the relevant mean and anomalous components of velocity and temperature for each advection term (see left panels of Fig. 8).

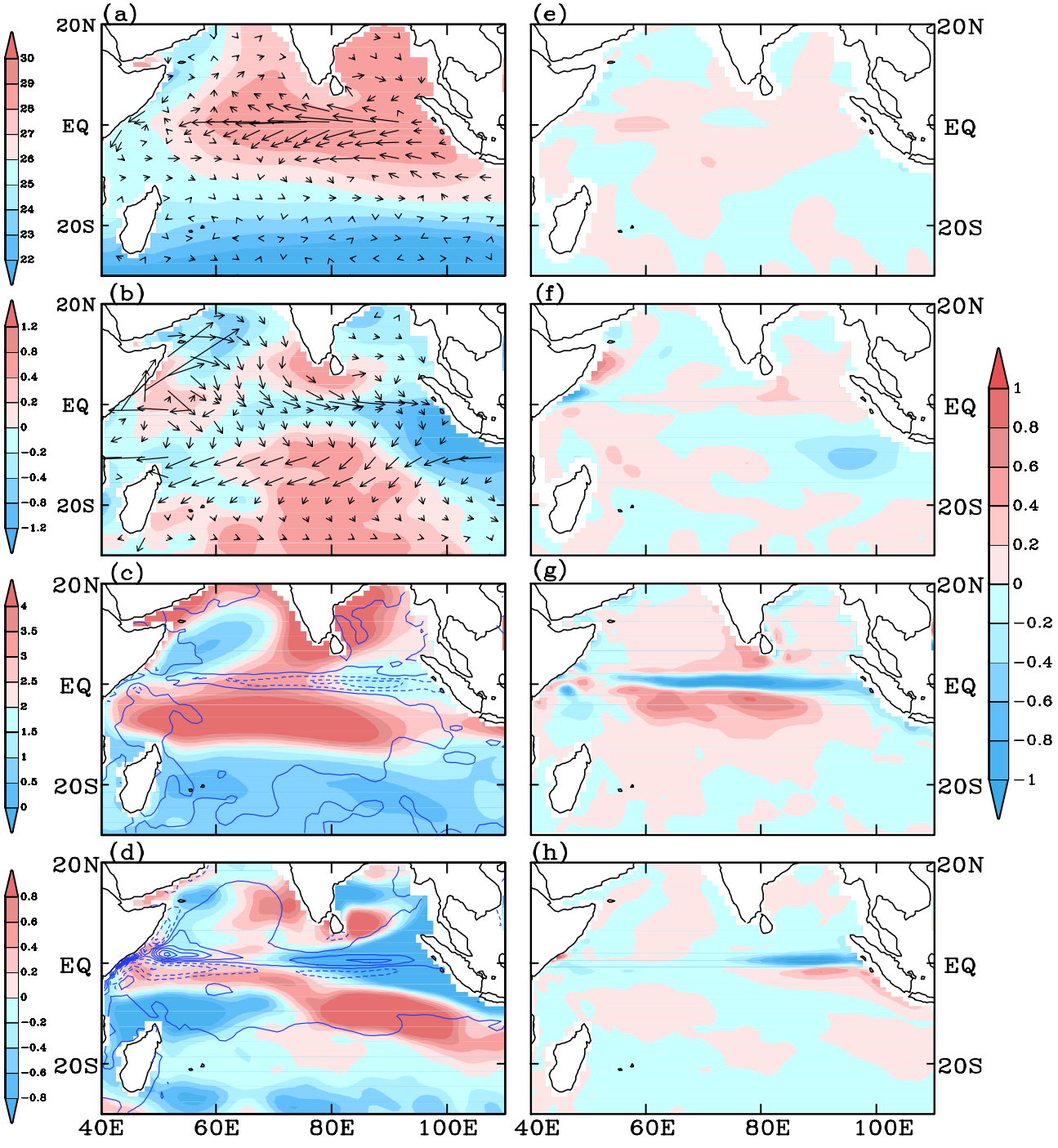

Fig. 8. July-August-September patterns of (a) anomalous horizontal ocean currents (arrows; units: m s^{-1}) and climatological temperature (shading; units: °C), (b) climatological horizontal ocean currents (arrows; units: m s^{-1}) and anomalous temperature (shading; units: °C), (c) anomalous oceanic upwelling speed (contours, interval: 10^{-6} m s^{-1}; units: m s^{-1}) and climatological vertical temperature stratification (shading; units: °C $month^{-1}$), and (d) climatological oceanic upwelling speed (contours, interval: 5×10^{-6} m s^{-1}; units: m s^{-1}) and anomalous vertical temperature stratification (shading; units: °C $month^{-1}$). Shown in (e)–(f) are the various components of temperature advection [$-\boldsymbol{V}' \cdot \nabla \overline{T}$, $\overline{\boldsymbol{V}} \cdot \nabla T'$, $W' \partial \overline{T} / \partial z$, and $\overline{W} \partial T' / \partial z$; see Eq. (2)], corresponding respectively to the patterns of the left panels. All are shown for the summer cold events. Units: °C $month^{-1}$.

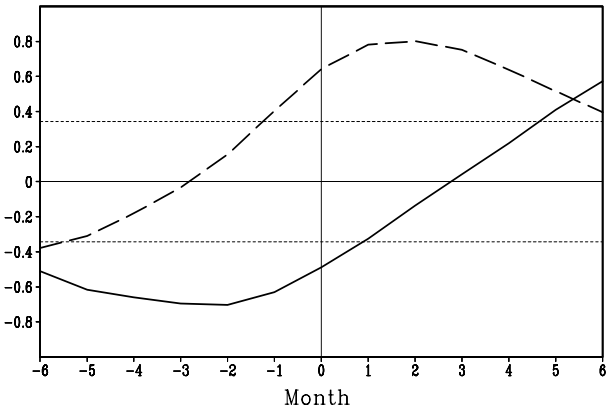

Fig. 9. Monthly lag correlation between the EIO index and Niño-3.4 index for summer (thick solid line) and winter (thick dashed line) events. Negative values in the x-coordinate represent the lead of the EIO to Niño-3.4. The thin dashed lines measure the significance at the 95% confidence level.

The most important advective processes in the tropical EIO are associated with the third term (Figs. 8c and 8g). The cooling tendency along the equatorial IO and the Sumatra and Java coasts is caused primarily by the anomalous equatorial and coastal upwelling of the background stratification. This upwelling is linked to the anomalous easterly and southeasterly surface winds off the Sumatra and Java coasts. When the easterly flow is strong enough to change the direction of total wind from easterly to westerly, the Wyrtki jet disappears or even reverses its direction, causing anomalous upwelling in the EIO. However, the fourth term, the background upwelling of anomalous stratification, appears to be compensative and potentially dominant along the coastline (Figs. 8d and 8h). Perhaps it is the combined effect of advection and upwelling that acts along the equator, while the second term dominates the southeastern region. The negative temperature anomalies produced by the anomalous temperature advection within (0°–15°S) may be attributed to the action of time-averaged current on the anomalous temperature gradient in the tropical southern IO (Figs. 8b and 8f).

Because of the enhancement of equatorial easterly anomalies caused by the anomalous anticyclonic winds over the southern IO, both the upwelling of deep cold water and the equatorward meridional advection increase (Webster et al., 1999; Murtugudde et al., 2000), which further cools the SST. Comparison among the results shown in Fig. 5 indicates that ocean temperature advection plays a stronger role for the summer cold events than for the others in cooling the EIO SST and in postponing the recovery of SST to normal conditions.

5. Relationship between Indian Ocean SST and ENSO

Saji et al. (1999) pointed out that the simultaneous correlation between the EIO and Niño-3.4 SSTs was weak (< 0.35 for 1958–99). However, Fig. 9 shows that the correlation coefficient is much higher (about -0.7) for the 10 summer cold and warm events during the seven-month lifespan when the EIO leads Niño-3.4 by two months (solid line). For winter, the highest correlation ($R = 0.8$) appears when Niño-3.4 leads the EIO by three months for the six-month lifespan in the 11 events (dashed line). That is, a strong relationship exists between EIO SST and ENSO at least for the selected summer and winter events. These corrections are statistically significant exceeding the 95% confidence level of the Student t-test for the number of the sample size.

Figure 10 shows the correlation between the EIO SST and grid-point SSTs and the regression of 850-hPa winds against EIO SST for the summer and winter events. The features for summer shown in Fig. 10a are similar to those of the first mode of the combined extended EOF analysis of surface winds, SST, and precipitation for the ENSO developing phase (SON; results not shown). Strong correlation appears not only over the tropical EIO, but also over the maritime continent and the western tropical Pacific. The correlation over the tropical western-central IO and central-eastern Pacific is opposite to that over the abovementioned regions. A pair of anomalous anticyclonic patterns appears over both hemispheres of the Indian Ocean and easterly anomalies occur along the equator corresponding to the atmospheric Rossby wave excited by the reduction of convection over the maritime continent. Meanwhile, a pair of anomalous cyclonic patterns appear over the tropical northwestern Pacific and central-southern Pacific. Correspondingly, westerly anomalies occur along the equator associated with the enhancement of convection over the central Pacific (Rasmusson and Wallace, 1983; Soman and Slingo, 1997; Krishnamurthy and Kirtman, 2003), consistent with the features shown in Fig. 4.

The winter events are characterized by basin-wide uniform SST anomalies in the tropical IO and a horseshoe pattern of SST anomalies in the tropical Pacific (Fig. 10b). Low-level anticyclonic wind anomalies appear over the Philippine Sea and westerly anomalies along the equatorial Pacific, shrunken to the central and eastern Pacific, in a pattern identical to the mature (DJF) and decay (MAM) phases of ENSO.

It is also shown by a combined extended EOF analysis that the atmospheric Rossby wave over the EIO is key for the development of the summer cold and

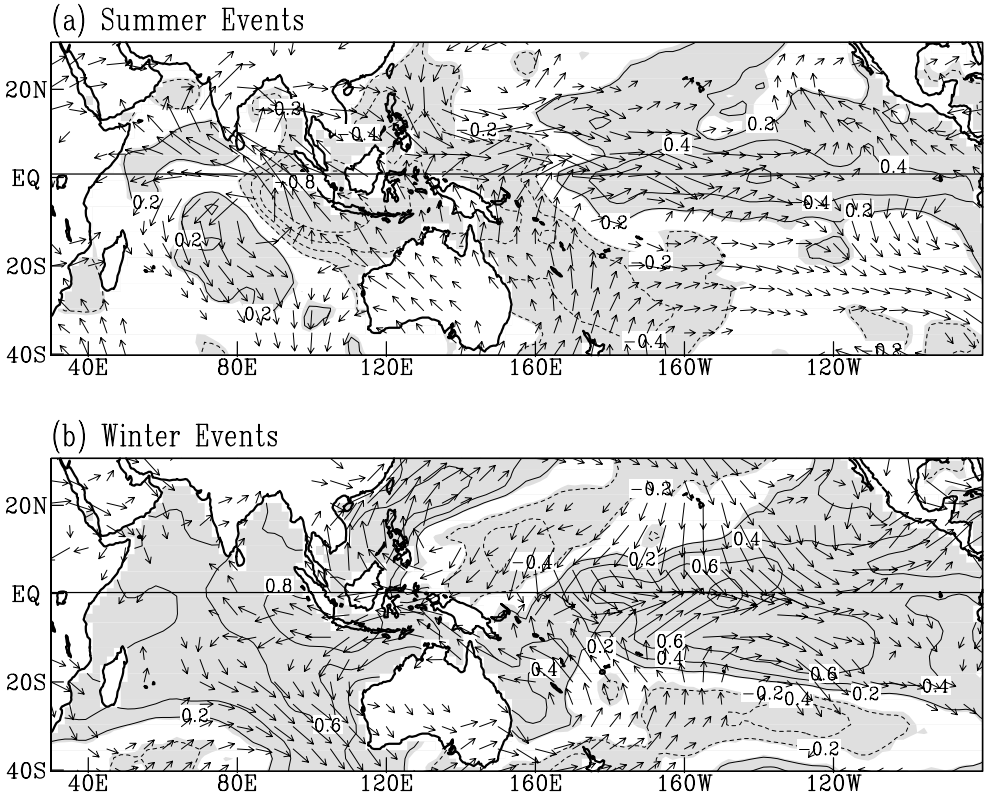

Fig. 10. Correlation of SST with the EIO index (contours) and regression of 850-hPa winds against the EIO index (vectors) for (a) summer events and (b) winter events. The shading areas indicate the significant SST-EIO correlation above the 95% confidence level.

warm events. The reduction (enhancement) of convection over the maritime continent is linked to the increase (decrease) in precipitation over the equatorial central-eastern Pacific through the Walker circulation when El Niño (La Niña) develops. Under this condition, the summer cold (warm) events in the EIO lead the El Niño (La Niña) mature phase by three months. However, if the changes in convection over the maritime continent are caused by other factors, the cold (warm) events may not correspond to El Niño (La Niña) closely, as in the cold event of 1961.

Because of the effects of ENSO and the Asian monsoon, the relationship between EIO SST and ENSO is complex. For example, if La Niña conditions follow an El Niño event, the winter and summer warm events tend to be combined into one event that may have double peaks. Thus, cold or warm events can be either suppressed or absorbed in the case of canonic ENSO events. Furthermore, the Asian monsoon varies strongly in both amplitude and locations, as seen in the variability of the monsoon-related buffer zone.

Figure 11 displays the positions of the buffer zone ($U = 0$) over the equatorial IO for the summer cold events (thick solid lines) and for the El Niño years without strong cooling in the EIO (thick dashed lines; for 1957, 1965, 1972, and 1982). The thin contours represent the climatological zonal surface wind and the thick black line indicates the climatological position of the summer monsoon buffer zone. On average, the monsoon buffer zone shifts to the north of the equator in most of the summer cold events, giving easterly wind along the equator. This shift exerts a strong influence on the Wyrtki jet and enhances the upwelling of cold water. The Wyrtki jet is in a narrow band, between 2°N and 2°S, and usually produces strong downwelling near the equatorial EIO (Wyrtki, 1973). If the easterly flow along the equator is strong enough to weaken or reverse the current of the jet, upwelling could bring the colder deep water to the surface and generate a strong cold event in the EIO, as in 1994 and 1997.

The last point that should be discussed is the distinct decadal variation of EIO SST and its relationship with ENSO (refer to Fig. 1). During the period of 1990–99, almost all events peak and are phase-locked in JJA or SON (summer events). Apart from the 1973 summer event, which may be an extension of the 1972–73 winter event, the entire period of 1965–90 is charac-

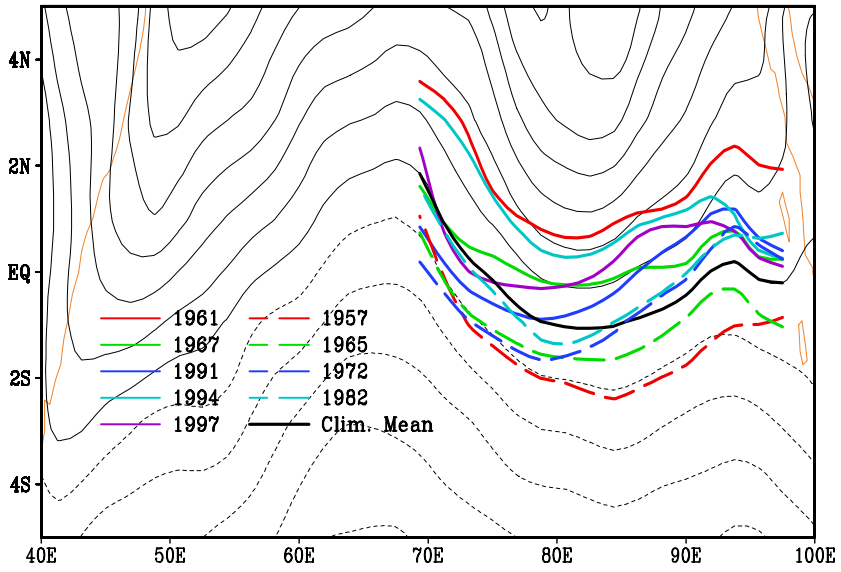

Fig. 11. Locations JJA buffer zone ($U = 0$; thick lines) for the summer cold events (solid lines) and for the El Niño years without strong cooling in the EIO (dashed lines). The thin contours (in intervals of 1 m s^{-1}) measure the zonal component of climatological surface winds.

terized by phase-locked peaks in DJF or MAM (winter events). A further look into this decadal variation indicates a change in phase with respect to Niño-3.4 SST. During the early period, the EIO and Niño-3.4 SSTs are positively correlated (0.4). However, in the latter period, they are negatively correlated (−0.7). This distinct change between the two periods is important for interpreting the apparently low correlation found by Saji et al. (1999) and others, which may point to a fundamentally different IO-ENSO relationship that necessitates further investigation.

6. Summary and discussion

In this study, we have focused on the physical characteristics of the cold and warm events observed in the EIO. These events, whose peaks are phase-locked with seasons, fully develop in the boreal summer or fall (summer events) and the boreal winter or early spring (winter events). We have examined the detailed features of these events by analyzing the variability in SST, surface winds, precipitation, and heat fluxes. In the summer cold (warm) events, cold (warm) SST anomalies appear in the tropical EIO and warm (cold) SST anomalies in the central-southern IO and WIO. However, the winter cold and warm events are characterized by uniform SST anomalies in the tropical IO. We have demonstrated that these EIO events are mainly caused by the easterly anomalies near the equator, through the air-sea interaction and the oceanic dynamics in which an atmospheric Rossby wave induced by the change in convection over the maritime continent interacts with different background monsoon flows. When the convection decreases (increases), cold (warm) events occur in the boreal summer and fall before the El Niño (La Niña) mature phase, and warm (cold) events appear in the boreal winter and spring after the El Niño (La Niña) mature phase.

As discussed above, the variability of EIO SST is mainly affected by the change in convection over the maritime continent and the Asian monsoon. Signals appear initially in the convection over the maritime continent, although these convection signals themselves may be linked to ENSO and other factors. Local air-sea interactions associated with the summer monsoon and oceanic process favor the development of summer events. When the convection decreases (increases) persistently, warm (cold) SST anomalies develop in winter through the air-sea interaction under the winter monsoon background. Perhaps, some summer cold (warm) events are not followed by El Niño (La Niña) because the developing El Niño (La Niña) conditions are interrupted or become weaker over the Pacific. However, winter warm (cold) events do depend strongly on major El Niño (La Niña) events to suppress convection until the next spring.

Figure 12 summarizes schematically a mechanism for summer cold events in which the interaction between the atmospheric Rossby wave and the summer monsoon is essential. When the convection over the maritime continent decreases and shifts eastward in the El Niño developing years, a pair of descending at-

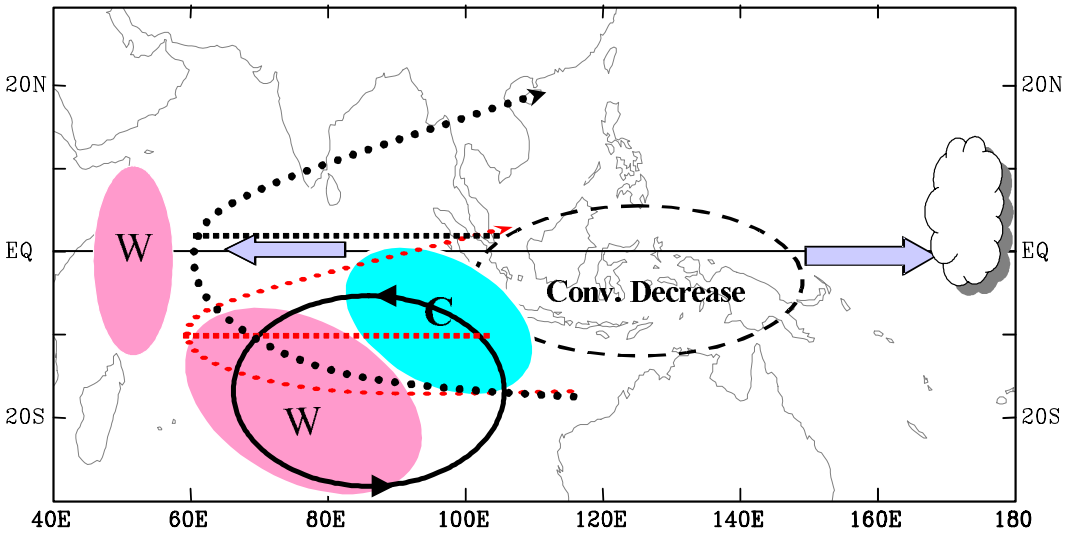

Fig. 12. Schematic diagram illustrating the mechanism for summer cold events through the interaction between the atmospheric Rossby wave and SST under the background of summer monsoon. The grey ovals represent warm (cold) SST anomalies, marked by W and C, respectively. The solid black lines with arrows represent the low-level anomalous anticyclonic Rossby wave over the southern IO, excited by the decreased convection over the maritime continent (dashed black line). The thick arrows measure the anomalous surface winds over the equator. The dotted black line with an arrow indicates the background flow of summer monsoon and the buffer zone position (straight, dashed black line), which shift southward in winter (grey dotted line with an arrow and the straightly-dashed line).

mospheric Rossby waves (anticyclones) is formed at the lower troposphere over the southern and northern IO, respectively. The southern one is stronger than the northern counterpart because of the stronger wind shear (Wang and Xie, 1997). Meanwhile, the easterly anomalies along the equator intensify the monsoon gyre to the south of the monsoon buffer zone, cooling the sea surface by the enhanced latent heat flux. These wind anomalies also weaken the Wyrtki jet and result in upwelling and further cooling in the EIO.

Towards the boreal winter, the same wind anomalies exert a different effect on SST due to the change in the basic monsoon flow. The easterly anomalies are now against the westerly basic flow along the equator and thus reduce latent heat flux. Also, because of the anomalous anticyclone, both solar radiation and SST increase rapidly over the EIO. Two to three months after the El Niño mature phase, the anomalous SST pattern is characterized by a uniform warming in the tropical IO. During the developing and decaying phases of La Niña, the above processes can be described correspondingly by signals of opposite signs.

Despite the IOD having been discussed extensively during recent years, controversies still remain surrounding its existence, its independence from ENSO, and its climate impact. Saji et al. (1999) were particularly interested in the basin-wide dipole as they attempted to link it with the severe rainfall events in East Africa. However, many of the strong signals appeared to emanate from the eastern IO, which is the focus of our present investigation. The summer cold events identified in this study are the cases of 1961, 1991, 1994, and 1997. Except for 1991, they are the dipole mode events studied by Saji et al. (1999). However, although the cold SST pattern in the EIO is similar to that shown by the previous study, the warm SST anomalies in the southern IO are much more robust than those in the WIO. Also, we have classified the 1967 event as an early spring cold event (in 1968) because the maximum SST anomalies appeared in DJF.

A greater argument surrounds the independence of the dipole mode from the ENSO signal. Although the full IOD time series has a low correlation of about -0.3 with Niño-3 SST, Allan et al. (2001) showed that the correlation between seasonally-stratified time series is much stronger (e.g., 0.56 for SON). The authors also showed that the IOD has a consistent relationship with SOI (-0.56) and the sea level pressure in Darwin (0.69). Our analysis has only provided preliminary results about the seasonal phase-locking of the warm and cool events in the EIO. In our composite analysis, the criterion of one standard deviation is arbitrary. It seems small for the recent events in the 1990s; how-

ever, a criterion of larger values would eliminate all but the most recent events. Using our criterion permits several marginal events such as the 1962 summer and 1966 and 1968 winter events that could bias the composite results to a certain extent. However, we have addressed this issue carefully by examining the composite patterns in which the weak events such as 1961 and 1962 summer events (see Figs. 1 and 2) are excluded and found that the main features shown in the composite patterns remain largely similar. In addition, we have found that our results are not dominated by the features associated with the strong events, like the 1987 winter and 1997 summer events.

The features of ocean-atmosphere interaction over the IO are determined not only by ENSO and the Asian monsoon but also by the local air-sea interaction and oceanic dynamic process (Huang and Kinter, 2002; Han et al., 2004). Recently, Shinoda et al. (2004) showed a subsurface dipole that might be more independent from ENSO, compared to the SST signal associated with the IOD. Discussions of this subsurface dipole are beyond the scope of this study, and the scenario proposed here for the relationship between the EIO cold/warm events and ENSO is highly idealized. A better understanding of the physical mechanisms for the features shown by this study should be improved by properly-designed experiments with coupled general circulation models.

Acknowledgements. The first author thanks Prof. B. Wang of the University of Hawaii for his support to the early stage of this study and many insightful discussions. Drs. Kyong-Hwan Seo and Y. Xue provided a number of helpful comments on an early version of the paper. The authors are grateful to the two anonymous reviewers who provided helpful suggestions leading to the improvement in the quality of this paper.

REFERENCES

Allan, R., and Coauthors, 2001: Is there an Indian Ocean dipole, and is it independent of the El Niño-Southern Oscillation? *CLIVAR Exchanges*, **6**, 18–22.

Anderson, D. L. T., and J. P. McCreary, 1985: On the role of the Indian Ocean in a coupled ocean-atmosphere model of El Niño and the Southern Oscillation. *J. Atmos. Sci.*, **42**, 2439–2442.

Baquero, A, M. Latif, and S. Legutke, 2002: On dipole like variability of sea surface temperature in the tropical Indian Ocean. *J. Climate*, **15**, 1358–1368.

Barnett, T. P., 1983: Interaction of the monsoon and Pacific Ocean trade wind systems at interannual time scales. Part I: the equatorial zone. *Mon. Wea. Rev.*, **111**, 756–773.

Bjerknes, J., 1969: Atmospheric teleconnections from the equatorial Pacific. *Mon. Wea. Rev.*, **97**, 163–172.

Cadet, D. L., 1985: The Southern Oscillation over the Indian Ocean. *J. Climate*, **5**, 189–212.

Carton, J. A., G. Chepurin, X. Cao, and B. Giese, 2000a: A simple ocean data assimilation analysis of the global upper ocean 1950–95. Part I: Methodology. *J. Phys. Oceanogr.*, **30**, 294–309.

Carton, J. A, G. Chepurin, and X. Cao, 2000b: A simple ocean data assimilation analysis of the global upper ocean 1950–95. Part II: Results. *J. Phys. Oceanogr.*, **30**, 311–326.

Chambers, D. P, B. D. Tapley, and R. H. Stewart, 1999: Anomalous warming in the Indian Ocean coincident with El Niño. *J. Geophys. Res.*, **104**, 3035–3047.

Chen, M., P. Xie, J. E. Janowiak, P. A. Arkin, and T. M. Smith, 2003: Reconstruction of the oceanic precipitation from 1948 to the present. *Proc. 14th Symposium on Global Changes and Climate Variations*, Long Beach, CA, 9–13.

Clarke, A. J., and X. Liu, 1993: Observations and dynamics of semiannual and annual sea levels near the eastern equatorial Indian Ocean boundary. *J. Phys. Oceanogr.*, **23**, 386–399.

Dommenget, D., and M. Latif, 2002: A cautionary note on the interpretation of EOFs. *J Climate*, **15**, 216–225.

Dommenget, D., and M. Latif, 2003: Reply. *J. Climate*, **16**, 1094–1097.

Gill, A. E., 1980: Some simple solutions for heat-induced tropical circulation. *Quart. J. Roy. Meteor. Soc.*, **106**, 447–446.

Han, W., P. Webster, R. Lukas, P. Hacker, and A. Hu, 2004: Impact of atmospheric intraseasonal variability in the Indian Ocean: low-frequency rectification in equatorial surface current and transport. *J. Phys. Oceanogr.*, **34**, 1350–1372.

Hastenrath, S., 2002: Temperature gradients, and tropical climate anomalies. *Bull. Amer. Meteor. Soc.*, **83**, 735–738.

Hastenrath, S., A. Nicklis, and L. Greischar, 1993: Atmospheric-hydrospheric mechanism of climate anomalies in the western equatorial Indian Ocean. *J. Geophys. Res.*, **98**, 20219–20235.

Huang, B. H., and J. L. Kinter, 2002: Interannual variability in the tropical Indian Ocean. *J. Geophys. Res.*, **107**, 3199, doi: 10.1029/2001JC001278.

Ju, J., and J. M. Slingo, 1995: The Asian monsoon and ENSO. *Quart. J. Roy. Meteor. Soc.*, **121**, 1133–1168.

Kalnay, E., and Coauthors, 1996: The NCEP/NCAR 40-year reanalysis project. *Bull. Amer. Meteor. Soc.*, **77**, 437–472.

Kiladis, G. N., and H. F. Diaz, 1989: Global climatic anomalies associated with extremes in the Southern Oscillation. *J. Climate*, **2**, 1069–1090.

Krishnamurthy, V., and B. P. Kirtman, 2003: Variability of the Indian Ocean: Relation to monsoon and ENSO. *Quart. J. Roy. Meteor. Soc.*, **129**, 1623–1646.

Latif, M., and T. P. Barnett, 1995: Interaction of the tropical oceans. *J. Climate*, **8**, 952–964.

Lau, N. C., and M. J. Nath, 1996: The role of the "at-

mospheric bridge" in linking tropical Pacific ENSO events to extratropical SST anomalies. *J. Climate*, **9**, 2036–2057.

Lau, N. C., and M. J. Nath, 2004: Coupled GCM simulation of atmosphere-ocean variability associated with zonally asymmetric SST changes in the tropical Indian Ocean. *J. Climate*, **17**, 245–265.

Loschnigg, J., G. A. Meehl, P. J. Webster, J. M. Arblaster, and G. P. Compo, 2003: The Asian Monsoon, the Tropospheric Biennial Oscillation, and the Indian Ocean Zonal Mode in the NCAR CSM. *J. Climate*, **16**, 1617–1642.

Meehl, G. A., 1997: The south Asian monsoon and the tropospheric biennal oscillation. *J. Climate*, **10**, 1921–1942.

Meyers, G., 1996: Variation of Indonesian throughflow and the El Niño-Southern Oscillation. *J. Geophys. Res.*, **101**, 12255–12263.

Murtugudde, R., and A. J. Busalachi, 1999: Interannual variability of the dynamics and thermodynamics of the tropical Indian Ocean. *J. Climate*, **12**, 2300–2326.

Murtugudde, R., J. P. McCreary, and A. J. Busalacchi, 2000: Oceanic process associated with anomalous events in the Indian Ocean with relevance to 1997–1998. *J. Geophys. Res.*, **105**, 3295–3306.

Nicholls, N., 1989: Predicting Indian monsoon rainfall from sea surface temperature in the Indonesian-north Australia area. *Nature*, **306**, 576–577.

Nicholson, S. E., 1997: An analysis of the ENSO signal in the tropical Atlantic and western Indian Oceans. *International Journal of Climatology*, **17**, 345–375.

Nigam, S., and H. S. Shen, 1993: Structure of atmospheric low-frequency variability over the tropical Pacific and Indian Ocean. Part I: COADS observations. *J. Climate*, **6**, 657–676.

Nitta, T., and S. Yamada, 1989: Recent warming of tropical sea surface temperature and its relationship to the Northern Hemisphere circulation. *J. Meteor. Soc. Japan*, **67**, 375–383.

Potemra, J., and R. Lukas, 1999: Seasonal to interannual modes of sea level variability in the western Pacific and eastern Indian Oceans. *Geophys. Res. Lett.*, **26**, 365–368.

Rasmusson, E. M., and J. M. Wallace, 1983: Meteorological aspects of the El Niño/Southern Oscillation. *Science*, **222**, 1195–1202.

Reynolds, R. W., and T. M. Smith, 1994: Improved global sea surface temperature analyses. *J. Climate*, **7**, 929–948.

Saji, N. H., and T. Yamagata, 2003: Structure of SST and surface wind variability during Indian Ocean dipole mode events: COADS observations. *J. Climate*, **16**, 2735–2751.

Saji, N. H., B. N. Goswami, P. N. Vinayachandran, and T. Yamagata, 1999: A dipole mode in the tropical Indian Ocean. *Nature*, **401**, 360–363.

Shinoda, T., H. H. Hendon, and M. A. Alexander, 2004: Surface and subsurface dipole variability in the Indian Ocean and its relation with ENSO. *Deep Sea Res.*, **51**, 619–635.

Shukla, J., 1987: Interannual variability of monsoons. *Monsoons*, J. S. Fein and P. L. Stephens, Eds., Wiley and Sons, 399–463.

Soman, M. K., and J. M. Slingo, 1997: Sensitivity of the Asian summer monsoon to aspects of sea-surface-temperature anomalies in the tropical Pacific Ocean. *Quart. J. Roy. Meteor. Soc.*, **123**, 309–336.

Tourre, Y. M., and W. B. White, 1995: ENSO signals in global upper-ocean temperature. *J. Phys. Oceanogr.*, **25**, 1317–1332.

Venzke, S., M. Latif, and A. Villwock, 2000: The coupled GCM ECHO-2. Part II: Indian Ocean response to ENSO. *J. Climate*, **15**, 1371–1383.

Wang, B., and X. Xie, 1997: A model for the boreal summer intraseasonal oscillation. *J. Atmos. Sci.*, **54**, 72–86.

Wang, B., and Q. Zhang, 2002: Pacific-East Asian teleconnection. Part II: How the Philippine Sea anomalous anticyclone is established during El Niño development. *J. Climate*, **15**, 3252–3265.

Wang, B., R. Wu, and X. Fu, 2000: Pacific-East Asian teleconnection: How does ENSO affect East Asian climate? *J. Climate*, **13**, 1517–1536.

Wang, B., R. Wu, and T. Li, 2003: Atmosphere-warm ocean interaction and its impacts on Asian-Australian monsoon variation. *J. Climate*, **16**, 1195–1211.

Webster, P. J., A. M. Moore, J. P. Loschnigg, and R. R. Leben, 1999: Coupled ocean-atmospheric dynamics in the Indian Ocean during 1997–98. *Nature*, **401**, 356–360.

Wolter, K., and S. Hastenrath, 1989: Annual cycle and long-term trends of circulation and climate variability over the tropical oceans. *J. Climate*, **2**, 1329–1351.

Wu, G. X., and W. Meng, 1998: Gearing between the Indo-monsoon circulation and the Pacific-Walker circulation and ENSO, I: Observation. *Chinese J. Atmos. Sci.*, **22**, 470–480. (in Chinses)

Wyrtki, K., 1973: An equatorial jet in the Indian Ocean. *Science*, **181**, 262–264.

Wyrtki, K., 1987: Indonesian through flow and the associated pressure gradient. *J. Geophys. Res.*, **92**, 12941–12948.

Xie, S. P, H. Annamalai, F. A. Schott, and J. P. McCreary, 2002: Structure and mechanisms of south Indian Ocean climate variability. *J. Climate*, **15**, 864–878.

Yamagata, T., K., Mizuno, and Y. Masumoto, 1996: Seasonal variations in the equatorial Indian Ocean and their impact on the Lombok throughflow. *J. Geophys. Res.*, **101**, 12465–12473.

Yamagata, T., S. K. Behera, S. A. Rao, Z. Guan, K. Ashok, and H. N. Saji., 2003: Comments on "Dipoles, temperature gradients, and tropical climate anomalies". *Bull. Amer. Meteor. Soc.*, **84**, 1418–1422.

Yang, S., X. Ding, D. Zheng, and S.-H. Yoo, 2007: Time-

frequency characteristics of the relationships between tropical Indo-Pacific SSTs. *Adv. Atmos. Sci.*, **24**(3), 343–359.

Yoo, S.-H., S. Yang, and C.-H. Ho, 2006: Variability of the Indian Ocean sea surface temperature and its impacts on Asian-Australian monsoon climate. *J. Geophys. Res.*, **111**, D03108, doi: 10.1029/2005JD006001.

Yu, L., and M. M. Rienecker, 1999: Mechanisms for the Indian Ocean warming during 1997–1998 El Niño. *Geophys. Res. Lett.*, **26**, 735–738.

Yu, J. Y., S. P. Weng, and J. D. Farrara, 2003: Ocean Roles in the TBO transitions of the Indian-Australian monsoon system. *J. Climate*, **16**, 3072–3080.